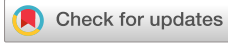


RESEARCH ARTICLE | SEPTEMBER 11 2023

Design and analysis of the power-trigonometric function-shaped flexure hinges

Jiabiao Li ; Yang Zhao  ; Qingwen Wu ; Peng Yu; Kai Zhang; Along Mao

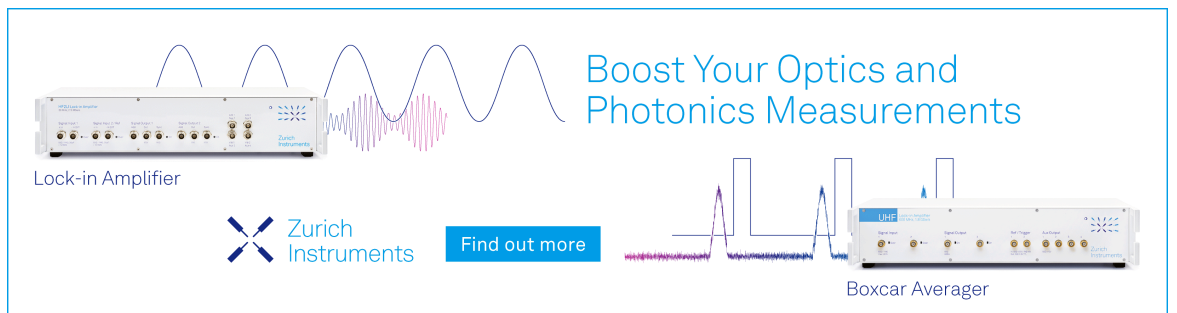


Rev. Sci. Instrum. 94, 095105 (2023)

<https://doi.org/10.1063/5.0154825>



CrossMark



Boost Your Optics and Photonics Measurements

Lock-in Amplifier

 [Find out more](#)

Boxcar Averager

Design and analysis of the power-trigonometric function-shaped flexure hinges

Cite as: Rev. Sci. Instrum. 94, 095105 (2023); doi: 10.1063/5.0154825

Submitted: 16 April 2023 • Accepted: 20 August 2023 •

Published Online: 11 September 2023



View Online



Export Citation



CrossMark

Jiabiao Li,^{1,2} Yang Zhao,^{1,2,a)} Qingwen Wu,^{1,2} Peng Yu,¹ Kai Zhang,¹ and Along Mao¹

AFFILIATIONS

¹Changchun Institute of Optics, Fine Mechanics and Physics, Chinese Academy of Sciences, Changchun 130033, China

²University of Chinese Academy of Sciences, Beijing 100049, China

^{a)}Author to whom correspondence should be addressed: zhaoyang9185@163.com

ABSTRACT

In this paper, a generalized flexure hinge model, that is, power-trigonometric function-shaped flexure hinges (PTFHs), is proposed. The power function and trigonometric function in the curve function are changed, which obtains different notch types of flexure hinges to meet the needs of flexure hinges in different scenarios. For the flexure hinge model, the notch curve equation of the hinge is presented first, and the influence of the degree of power function, degree of trigonometric function, and other parameters on the structure of the curve is analyzed. Then, the compliance and rotation precision equations of the flexure hinge are derived based on Castigliano's second theorem. Both equations are verified using the finite element method and achieve errors of less than 8.5%. Then, based on the flexure hinge equation, the influence of the size parameters on the compliance and rotation precision of the hinge is analyzed, and a new comparison method is proposed. Parameter β is defined to analyze the influence of five parameters on β . Through the comparison of PTFHs and three commonly used flexure hinges, the results prove that the proposed PTFHs have better comprehensive performance. Then, the flexure hinge is statically analyzed. Finally, a test system for flexure hinges is established to verify the performance of the model.

Published under an exclusive license by AIP Publishing. <https://doi.org/10.1063/5.0154825>

I. INTRODUCTION

With the development of science and technology, compliant mechanisms have gradually become an indispensable part in many applications of high precision, sensitivity, and resolution motion.¹ Flexure hinges are the most important component of compliant mechanisms. Flexure hinges provide relative rotation between adjacent rigid members by buckling, unlike traditional rotating joints. Each individual flexure hinge should have a complete set of compliant mechanisms to define its mechanical response under static loading.^{2,3} A flexure hinge has the advantages of compact structure, small volume, no gap, no friction, no lubrication, smooth and continuous motion, and high displacement resolution,^{4–7} which make it widely used in positioning vibration isolation tables,⁸ precision positioning,^{9,10} microgrippers,¹¹ spring constant calibration systems,¹² microelectromechanical systems (MEMS),¹³ driving mechanisms,¹⁴ and other fields.^{15–18}

Various types of flexure hinges have been studied. Paros *et al.*¹⁹ studied circular flexure hinges first and then proposed theoretical calculation formulas. Lobontiu *et al.*²⁰ used Castigliano's second

theorem to compare the compliance of circular, elliptical, hyperbolic, and parabolic flexure hinges and concluded that the elliptical flexure hinge has better compliance and the hyperbolic flexure hinge has better rotation precision. Tian *et al.*²¹ proposed a new type of rounded V-shaped flexure hinge and derived the compliance equation and rotation precision equation. Lin *et al.*²² designed a hybrid flexure hinge that included a hyperbolic flexure hinge and corner-tilted flexure hinge. Liu *et al.*²³ designed a quasi-V-shaped flexure hinge using topology optimization, which has higher rotation precision than the rounded V-shaped flexure hinge but lower compliance. Li *et al.*²⁴ proposed a power function-type flexure hinge, which has higher rotation precision than the straight circular flexure hinge and V-shaped flexure hinge. Wei *et al.*²⁵ proposed elliptic-revolute notch type multiple-axis flexure hinges and then provided closed-form compliance equations. Wang *et al.*²⁶ proposed a new exponential-sine-shaped flexure hinge with an asymmetric structure and used a novel finite beam matrix modeling method to calculate the compliance matrix and the rotation precision matrix. Wu *et al.*²⁷ proposed a new conical notch flexure hinge compliance analytical model, which uses non-uniform rational B-spline curves to

parameterize the flexure hinge. The curve can describe various notch types, such as ellipse, parabola, and hyperbola. Chen *et al.*²⁸ proposed a universal model that can be applied to circles, ellipses, and right-circular shapes by changing the parameters. Li *et al.*² presented a method based on a generalized analytical compliance matrix to establish compliance and rotation precision equations for mixed bending hinges. This model can also handle the complex shapes of hinges. Kong *et al.*²⁹ proposed a generalized model called the conic V-shaped flexure hinge, which can achieve parabolic V-shaped, elliptical V-shaped, and hyperbolic V-shaped transformations by changing parameters. Li *et al.*³⁰ also proposed two universal models that can quickly establish compliance and rotation precision equations for multi-axis flexure hinges. Wei *et al.*³¹ introduced a mixed multi-axis flexure hinge with a generalized elliptical-arc hybrid corner notch contour and studied the effects of parameters on it. Lin *et al.*³² reported a new notch flexure hinge with adjustable curvatures and, through the theory and a finite element calculation, found that it had high rotation accuracy.

Most forms of flexure hinges are unchanged, that is, they are composed of a single conic curve or two or more conic curves combined, or they are composed of a certain form of function. Therefore, in this paper, a new type of flexure hinge, called the power-trigonometric function-shaped flexure hinge (PTFH), is proposed, which is used to develop a general flexure hinge model. PTFHs are bending hinges with new notch-type flexure hinges that have different notch types that can be obtained by changing the degree of power function and trigonometric function in the PTFHs' curve function.

This paper is organized as follows: in Sec. II, the curve equation and structural characteristics of the PTFH are introduced. Then, in Sec. III, the compliance and rotation precision equations of PTFHs are derived and verified using the finite element method, the influence of structural parameters on compliance and rotation precision is analyzed, a new comparison method is provided to enable the selection of better structural parameters, and PTFHs are compared with three commonly used flexure hinges. In Sec. IV, the strength and displacement space are analyzed using the finite element method. Then, in Sec. V, experimental analysis is performed to verify the correctness of the analysis and design. Finally, in Sec. VI, the study is summarized.

II. FLEXURE HINGE DESIGN

Figure 1 shows a schematic structural diagram of the PTFH, where L is the total length of the flexure hinge, l is the length of the notch, d is the minimum thickness of the notch, D is the diameter of the flexure hinge, and a is the cylindrical part of the flexure hinge length. The curve of the flexure hinge can be described as follows:

$$y = -m \times \left(\frac{x}{n}\right)^q \times \cos^u\left(\frac{x}{n}\right) - z + \frac{d}{2}, \quad 0 \leq x \leq l, \quad (1)$$

$$z = \min\left(-m \times \left(\frac{x}{n}\right)^q \times \cos^u\left(\frac{x}{n}\right)\right). \quad (2)$$

Generally, the rotation center is defined as the center of the cross section where the thickness is minimum. Regarding the

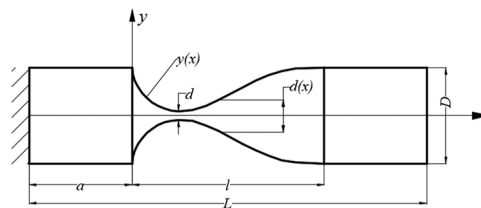


FIG. 1. Theoretical architecture model of flexure hinge.

flexure hinge, the rotation center can be determined according to the following equation:

$$\begin{aligned} \frac{\partial y}{\partial x} &= -m \times q \times \left(\frac{x}{n}\right)^{q-1} \cos^u\left(\frac{x}{n}\right) \\ &+ m \times \left(\frac{x}{n}\right)^q \times u \times \frac{1}{n} \cos^{u-1}\left(\frac{x}{n}\right) \sin\left(\frac{x}{n}\right), \\ &= 0, \end{aligned} \quad (3)$$

where m and n denote the depth factor and length factor, respectively, and q and u , respectively, denote the degree of power function and degree of the trigonometric function that govern the profile of the curve of the flexure hinge. The relationship between diameter d and m and the relationship between notch length l and n are given by

$$D = (x_1 \times m \times 2) + d, \quad (4)$$

$$z_1 = \min(-x^q \times \cos^u x), \quad (5)$$

where x_1 is the x value corresponding to z_1 and

$$l = n \times 0.5 \times \pi. \quad (6)$$

To gain an intuitive understanding of the influence of the four parameters m , n , q , and u on the curve of the flexure hinge, the following parameters are set to generate the profiles shown in Fig. 2:

- Set $n = 20$, $q = 0.5$, $u = 3$, and m ranges from 10 to 40.
- Set $m = 30$, $q = 0.5$, $u = 3$, and n ranges from 15 to 27.
- Set $l = 30$, $D = 20$, $u = 3$, and q ranges from 0.5 to 3.
- Set $l = 30$, $D = 20$, $q = 0.5$, and u ranges from 0.5 to 3.

III. THEORETICAL CALCULATION OF FLEXURE HINGES

A. Compliance calculation

The theoretical principle of flexure hinge is shown in Fig. 3, where point 2 indicates the ideal center of rotation and point 1 indicates the free end. The mechanical analysis model of an unsymmetrical conical flexure hinge is an Euler–Bernoulli beam with a small displacement, which is subjected to bending caused by external forces and bending moments. Simultaneously, the axial load is considered and the shear effect is not considered.

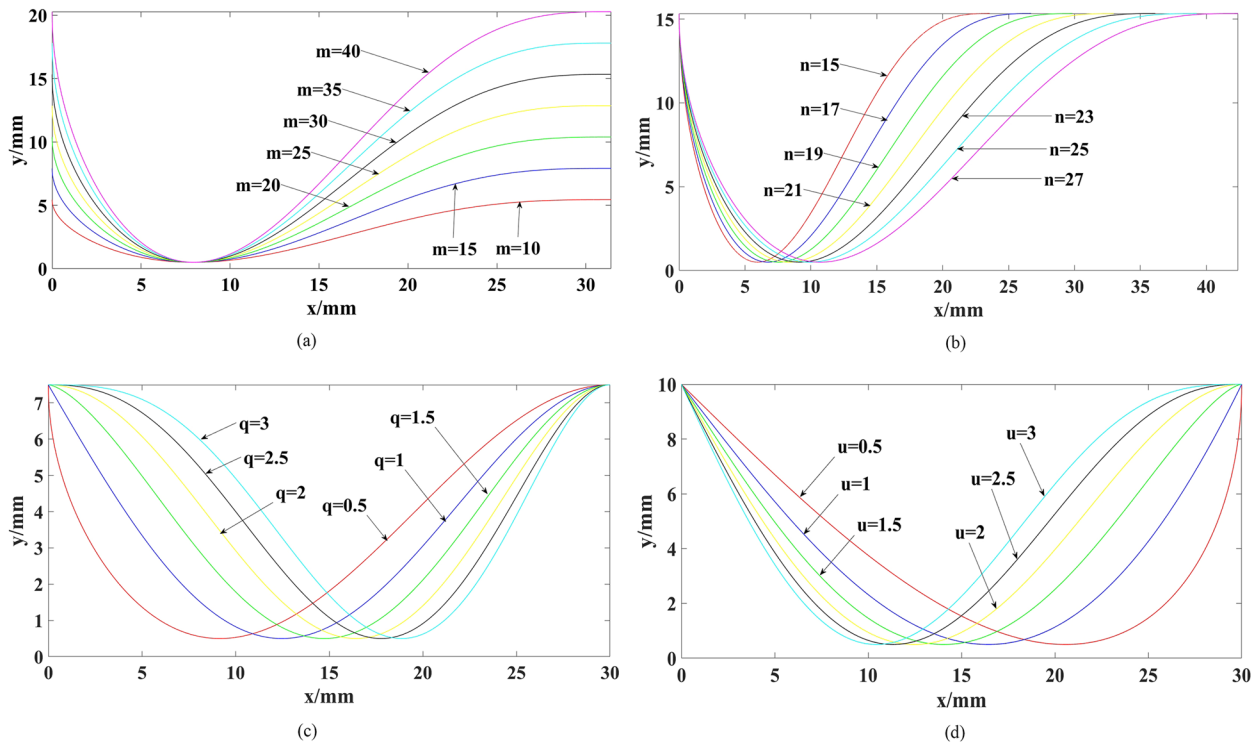


FIG. 2. Profiles of the flexure hinge. (a) Profiles of the flexure hinge in terms of m . (b) Profiles of the flexure hinge in terms of n . (c) Profiles of the flexure hinge in terms of q . (d) Profiles of the flexure hinge in terms of u .

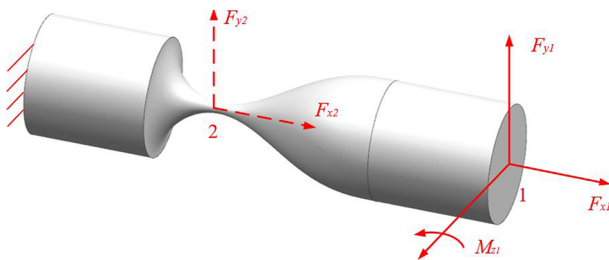


FIG. 3. Schematic of the flexure hinge with external forces.

Force vector T and deformation vector W are defined as follows:

$$\begin{cases} T = [F_{x_1}, F_{y_1}, M_{z_1}]^T, \\ W = [\Delta x_1, \Delta y_1, \Delta \theta_{z_1}]^T. \end{cases} \quad (7)$$

The following relationship can be obtained:

$$W = CT, \quad (8)$$

$$C = \begin{bmatrix} \frac{\Delta x_1}{F_{x_1}} & 0 & 0 \\ 0 & \frac{\Delta y_1}{F_{y_1}} & \frac{\Delta y_1}{M_{z_1}} \\ 0 & \frac{\Delta \theta_{z_1}}{F_{y_1}} & \frac{\Delta \theta_{z_1}}{M_{z_1}} \end{bmatrix}, \quad (9)$$

where C is a symmetric matrix. This yields the following relationship:

$$\frac{\Delta \theta_{z_1}}{F_{y_1}} = \frac{\Delta y_1}{M_{z_1}}. \quad (10)$$

According to Castigliano's second theorem,^{33,34}

$$\begin{cases} \Delta x_1 = \frac{\partial U}{\partial F_{x_1}}, \\ \Delta y_1 = \frac{\partial U}{\partial F_{y_1}}, \\ \Delta \theta_{z_1} = \frac{\partial U}{\partial M_{z_1}}. \end{cases} \quad (11)$$

According to the mechanics of materials, the deformation energy of the flexure hinge is as follows:

$$U = \frac{1}{2} \left(\int \frac{F_x^2}{EA(x)} dx + \int \frac{M_z^2}{EI_z(x)} dx \right), \quad (12)$$

$$F_x = F_{x_1}, M_z = M_{z_1} - F_{y_1}(L - x), \quad (13)$$

where E is the Young's modulus of the material, $A(x)$ is the cross-sectional area of the hinge, $d(x)$ is the variable thickness of the hinge, and $I_z(x)$ is the moment of inertia,

$$A(x) = \frac{\pi d^2(x)}{4}, \quad I_z(x) = \frac{\pi d^4(x)}{64}, \quad (14)$$

$$d(x) = \begin{cases} D, & -a < x < 0, \\ 2 \times \left(-m \times \left(\frac{x}{n}\right)^q \cos^u\left(\frac{x}{n}\right) - z + \frac{d}{2}\right), & 0 < x < l, \\ D, & l < x < L - a. \end{cases} \quad (15)$$

The compliance of the flexure hinge can be calculated from Eqs. (7)–(15) as follows:

$$\begin{aligned} \frac{\Delta\theta_{z1}}{M_{z1}} &= \frac{64}{\pi E} \int \frac{dx}{d^4(x)} = \frac{64}{\pi E} \left(\int_{-a}^0 \frac{dx}{D^4} + \int_0^l \frac{dx}{\left(2 \times \left(-m \times \left(\frac{x}{n}\right)^q \cos^u\left(\frac{x}{n}\right) - z + \frac{d}{2}\right)\right)^4} + \int_l^{L-a} \frac{dx}{D^4} \right), \\ \frac{\Delta\theta_{z1}}{F_{y1}} = \frac{\Delta y_1}{M_{z1}} &= -\frac{64}{\pi E} \int \frac{(L-x)dx}{d^4(x)} = -\frac{64}{\pi E} \left(\int_{-a}^0 \frac{(L-x)dx}{D^4} + \int_0^l \frac{(L-x)dx}{\left(2 \times \left(-m \times \left(\frac{x}{n}\right)^q \cos^u\left(\frac{x}{n}\right) - z + \frac{d}{2}\right)\right)^4} + \int_l^{L-a} \frac{(L-x)dx}{D^4} \right), \\ \frac{\Delta y_1}{F_{y1}} &= \frac{64}{\pi E} \int \frac{(L-x)^2 dx}{d^4(x)} = \frac{64}{\pi E} \left(\int_{-a}^0 \frac{(L-x)^2 dx}{D^4} + \int_0^l \frac{(L-x)^2 dx}{\left(2 \times \left(-m \times \left(\frac{x}{n}\right)^q \cos^u\left(\frac{x}{n}\right) - z + \frac{d}{2}\right)\right)^4} + \int_l^{L-a} \frac{(L-x)^2 dx}{D^4} \right), \\ \frac{\Delta x_1}{F_{x1}} &= \frac{4}{\pi E} \int \frac{dx}{d^2(x)} = \frac{4}{\pi E} \left(\int_{-a}^0 \frac{dx}{D^2} + \int_0^l \frac{dx}{\left(2 \times \left(-m \times \left(\frac{x}{n}\right)^q \cos^u\left(\frac{x}{n}\right) - z + \frac{d}{2}\right)\right)^2} + \int_l^{L-a} \frac{dx}{D^2} \right). \end{aligned} \quad (16)$$

B. Rotation precision

Different from traditional rigid hinges, flexure hinges have an ideal center of rotation that moves slightly during elastic deformation, which leads to parasitic motion that decreases rotation precision. When two fictitious loads are applied at point 2, the displacement vector Y is defined as follows:

$$Y = [\delta x_2, \delta y_2, 0]^T. \quad (17)$$

The displacement–load relationship can be obtained as follows:

$$Y = \begin{bmatrix} \frac{\delta x_2}{F_{x_1}} & 0 & 0 \\ 0 & \frac{\delta y_2}{F_{y_1}} & \frac{\delta y_2}{M_{z_1}} \\ 0 & 0 & 0 \end{bmatrix} \begin{bmatrix} F_{x_1} \\ F_{y_1} \\ M_{z_1} \end{bmatrix}. \quad (18)$$

Castigliano's second theorem is used again to determine the

displacements of the rotation center in the form of the flexure hinge,

$$\begin{cases} \delta x_2 = \frac{\partial U_e}{\partial F_{x_2}}, \\ \delta y_2 = \frac{\partial U_e}{\partial F_{y_2}}. \end{cases} \quad (19)$$

Again, bending and axial tension together constitute the elastic strain energy,

$$U_e = \frac{1}{2} \left(\int \frac{F_x'^2}{EA(x)} dx + \int \frac{M_z'^2}{EI_z(x)} dx \right), \quad (20)$$

$$F'_x = F_{x_1} + F_{x_2},$$

$$M'_z = M_{z_1} - F_{y_1}(L - x) - F_{y_2} \left(\frac{L}{2} - x\right). \quad (21)$$

Then, the rotation precision of the flexure hinge can be calculated from Eqs. (17)–(21) as follows:

$$\begin{aligned} \frac{\delta y_2}{M_{z1}} &= -\frac{64}{\pi E} \int_L \frac{(L_1 - x)}{d^4(x)} dx = -\frac{64}{\pi E} \left(\int_{-a}^0 \frac{(L_1 - x)dx}{D^4} + \int_0^l \frac{(L_1 - x)dx}{\left(2 \times \left(-m \times \left(\frac{x}{n}\right)^q \cos^u\left(\frac{x}{n}\right) - z + \frac{d}{2}\right)\right)^4} \right), \\ \frac{\delta y_2}{F_{y1}} &= \frac{64}{\pi E} \int_L \frac{(L-x)(L_1-x)}{d^4(x)} dx = \frac{64}{\pi E} \left(\int_{-a}^0 \frac{(L-x)(L_1-x)dx}{D^4} + \int_0^l \frac{(L-x)(L_1-x)dx}{\left(2 \times \left(-m \times \left(\frac{x}{n}\right)^q \cos^u\left(\frac{x}{n}\right) - z + \frac{d}{2}\right)\right)^4} \right), \\ \frac{\delta x_2}{F_{x1}} &= \frac{4}{\pi E} \int_L \frac{1}{d^2(x)} dx = \frac{4}{\pi E} \left(\int_{-a}^0 \frac{dx}{D^2} + \int_0^l \frac{dx}{\left(2 \times \left(-m \times \left(\frac{x}{n}\right)^q \cos^u\left(\frac{x}{n}\right) - z + \frac{d}{2}\right)\right)^2} \right). \end{aligned} \quad (22)$$

TABLE I. Parameters of the selected PFTH.

Number	q	u	m	n	d/mm
1	0.5	1	27	20	1.5
2	0.5	2	27	20	1.5
3	1	2	26	19	1.3
4	1	3	26	18	1.3
5	2	1.5	25	18	1
6	2	2.5	25	19	1
7	3	2	24	19	1
8	3	1.5	24	19	1

C. Finite element verification

To verify the compliance expressions shown in Eqs. (16) and (22), a finite element model was built to analyze the hinge. The flexure hinge’s C3D10 mesh model was created. The mesh’s average edge length was 1 mm. Detailed grids had to be created in the deformation area to obtain accurate results. The dimensional parameters chosen during the finite element analysis (FEA) and analytical modeling processes are listed in Table I. Young’s modulus and Poisson’s ratio were set to $E = 128\,000$ MPa and $\mu = 0.35$, respectively.

The planar compliances obtained by the two methods and used to verify the correctness of the expressions for describing the compliance and rotation precision of the flexure hinges are presented in Table II. The FEA results were considered as “accurate” values,

and then, the relative errors were calculated using the following equation:

The results are presented in Table II.

$$\text{Err} = \left| \frac{\text{FEA} - \text{Ana.}}{\text{FEA}} \right| \times 100\%. \quad (23)$$

The FEA and the method obtained using the analytical results are represented by Ana. and FEA, respectively. The relative errors are denoted by Err.% and were calculated using Eq. (23). As presented in Table II and Fig. 4, most of the relative errors were below 8.5% and the maximum relative error was ~8.421%. The results

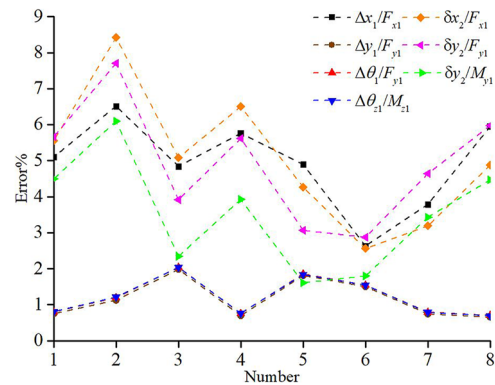


FIG. 4. Error curve of the theoretical analysis and FEA.

TABLE II. Comparison of the theoretical analysis and FEA.

		1	2	3	4	5	6	7	8
$\Delta x_1/F_{x_1}$ ($N^{-1} \text{ mm} \times 10^{-5}$)	Ana.	2.481	2.083	2.701	2.477	3.571	4.344	3.861	3.264
	FEA	2.615	2.228	2.839	2.628	3.755	4.461	4.013	3.47
	Err.%	5.103	6.516	4.846	5.759	4.899	2.636	3.788	5.953
$\Delta y_1/F_{y_1}$ ($N^{-1} \text{ mm} \times 10^{-1}$)	Ana.	2.054	1.23	1.63	1.553	2.376	3.647	2.482	1.874
	FEA	2.039	1.216	1.598	1.542	2.334	3.593	2.463	1.862
	Err.%	0.753	1.13	1.986	0.7	1.815	1.506	0.748	0.661
$\Delta \theta_1/F_{y_1}$ ($N^{-1} \times 10^{-3}$)	Ana.	4.736	3.343	5.021	4.644	9.061	12.205	9.486	7.66
	FEA	4.698	3.303	4.92	4.609	8.895	12.019	9.411	7.606
	Err.%	0.805	1.201	2.042	0.761	1.857	1.548	0.796	0.708
$\Delta \theta_{z_1}/M_{z_1}$ ($N^{-1} \text{ mm}^{-1} \times 10^{-4}$)	Ana.	1.093	0.91	1.549	1.391	3.46	4.092	3.633	3.135
	FEA	1.084	0.899	1.518	1.38	3.397	4.03	3.604	3.114
	Err.%	0.811	1.215	2.036	0.766	1.843	1.548	0.791	0.694
$\delta x_2/F_{x_1}$ ($N^{-1} \text{ mm} \times 10^{-5}$)	Ana.	1.215	0.988	1.324	1.189	1.841	2.185	2.009	1.723
	FEA	1.287	1.079	1.395	1.272	1.923	2.242	2.075	1.811
	Err.%	5.558	8.421	5.085	6.503	4.27	2.561	3.193	4.879
$\delta y_2/F_{y_1}$ ($N^{-1} \text{ mm} \times 10^{-3}$)	Ana.	2.902	1.646	2.499	2.033	3.767	5.922	4.27	2.992
	FEA	3.076	1.783	2.601	2.154	3.887	6.098	4.478	3.182
	Err.%	5.665	7.705	3.917	5.619	3.069	2.877	4.642	5.977
$\delta y_2/M_{y_1}$ ($N^{-1} \times 10^{-5}$)	Ana.	6.39	4.278	7.32	5.81	13.649	18.739	15.356	11.605
	FEA	6.691	4.556	7.496	6.048	13.873	19.083	15.902	12.148
	Err.%	4.499	6.098	2.346	3.927	1.612	1.802	3.433	4.47

indicate a good agreement between the FEA and the analytical results.

D. Performance analysis of flexure hinge

To design a flexure hinge that meets the design requirements efficiently, it is necessary to determine the relationship between the structural parameters of the flexure hinge and its compliance and rotation precision. Five parameters govern the shape of the flexure hinge: q , u , m , n , and d . If any parameter changes within a reasonable range and other parameters are fixed, compliance and rotation precision under various parameters can be obtained using formulas, and the influence of a parameter on compliance and rotation precision performance can be obtained.

To investigate the influence of q and u , the remaining parameters l , D , and d were assumed to be 30, 15, and 1 mm, respectively, whereas both q and u range from 0.5 to 3. The compliance and rotation precision obtained in terms of q and u are illustrated in Fig. 5. To investigate the influences of m and n , the remaining parameters q , u , and d were assumed to be 0.5, 3, and 1 mm, respectively, whereas m ranged from 14 to 20 and n ranged from 18 to 24. The compliance and rotation precision obtained in terms of m and n are illustrated in

Fig. 6. To investigate the influences of d , the remaining parameters q , u , D , and l were assumed to be 0.5, 3, 15, and 30 mm, respectively, whereas d ranged from 1.0 to 1.6 mm. The compliance and rotation precision obtained in terms of d are illustrated in Fig. 7.

From the relationships shown in Fig. 5, the compliances $\Delta x_1/F_{x_1}$, $\Delta \theta_1/F_{y_1}$, $\Delta \theta_1/F_{y_1}$, and $\Delta \theta_{z_1}/M_{z_1}$ and the rotation precision δ_{x_2}/F_{x_1} , δ_{y_2}/F_{y_1} , and δ_{y_2}/M_{z_1} decreased nonlinearly as parameter q increased. However, the trend of the compliance and rotation precision changes was not very clear with respect to variations of u .

From the relationships shown in Fig. 6, the compliances $\Delta x_1/F_{x_1}$, $\Delta y_1/F_{y_1}$, $\Delta \theta_1/F_{y_1}$, and $\Delta \theta_{z_1}/M_{z_1}$ and the rotation precision δ_{x_2}/F_{x_1} , δ_{y_2}/F_{y_1} , and δ_{y_2}/M_{z_1} increased nonlinearly as parameter m increased. The compliances $\Delta x_1/F_{x_1}$, $\Delta y_1/F_{y_1}$, $\Delta \theta_1/F_{y_1}$, and $\Delta \theta_{z_1}/M_{z_1}$ and the rotation precision δ_{x_2}/F_{x_1} , δ_{y_2}/F_{y_1} , and δ_{y_2}/M_{z_1} increased nonlinearly as parameter n increased.

From the relationships shown in Fig. 7, the compliances $\Delta x_1/F_{x_1}$, $\Delta y_1/F_{y_1}$, $\Delta \theta_1/F_{y_1}$, and $\Delta \theta_{z_1}/M_{z_1}$ and the rotation precision δ_{x_2}/F_{x_1} , δ_{y_2}/F_{y_1} , and δ_{y_2}/M_{z_1} decreased nonlinearly as parameter d increased.

Generally, changes to compliance and rotation precision follow opposite trends, that is, the greater the compliance, the lower

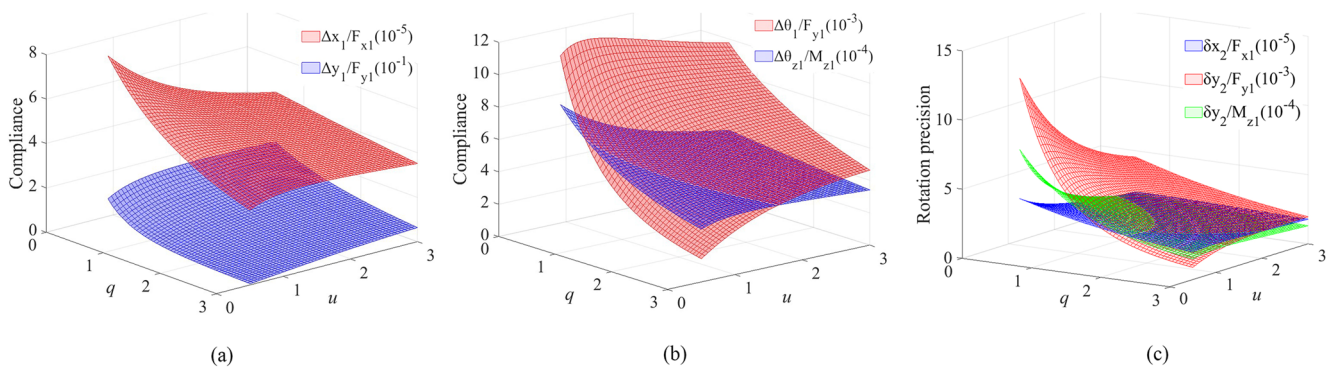


FIG. 5. Influence of geometric parameters q and u on PTFHs. (a) Compliance $\Delta x_1/F_{x_1}$ and $\Delta y_1/F_{y_1}$ of PTFHs. (b) Compliance $\Delta \theta_1/F_{y_1}$ and $\Delta \theta_{z_1}/M_{z_1}$ of PTFHs. (c) Rotation precision δ_{x_2}/F_{x_1} , δ_{y_2}/F_{y_1} , and δ_{y_2}/M_{z_1} of PTFHs.

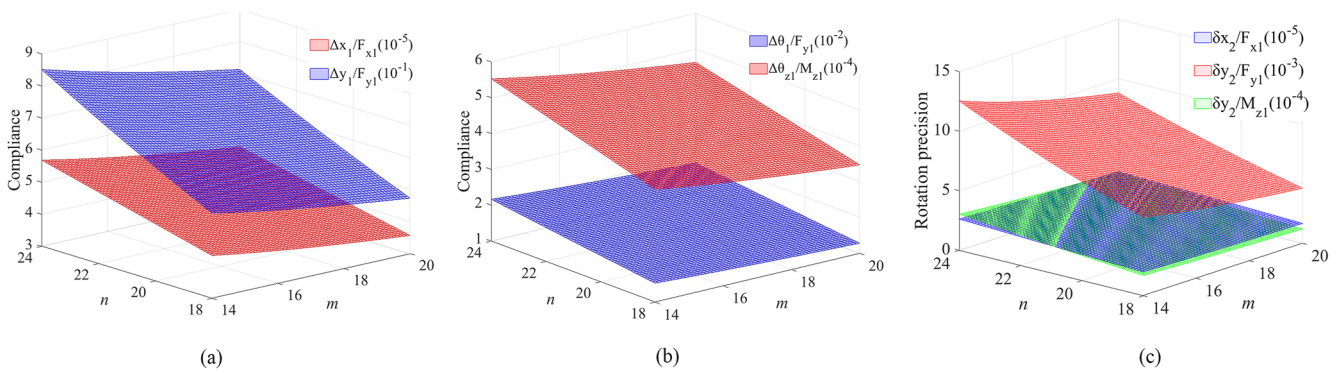


FIG. 6. Influence of geometric parameters m and n on PTFHs. (a) Compliance $\Delta x_1/F_{x_1}$ and $\Delta y_1/F_{y_1}$ of PTFHs. (b) Compliance $\Delta \theta_1/F_{y_1}$ and $\Delta \theta_{z_1}/M_{z_1}$ of PTFHs. (c) Rotation precision δ_{x_2}/F_{x_1} , δ_{y_2}/F_{y_1} , and δ_{y_2}/M_{z_1} of PTFHs.

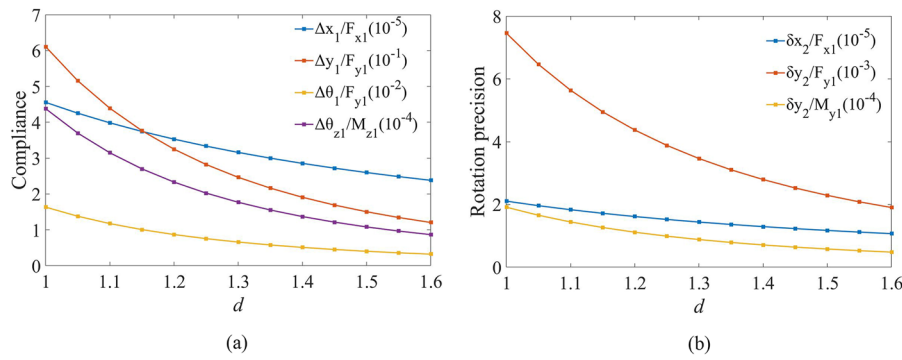


FIG. 7. Influence of geometric parameters d on PTFHs. (a) Compliance and (b) rotation precision.

the rotation precision; therefore, a single increase in compliance will lead to a reduction of rotation precision; to derive the overall performance of the flexure hinge, the following expressions are defined:

$$A = \frac{\Delta x_1}{F_{x1}} + \frac{\Delta y_1}{F_{y1}} + \frac{\Delta \theta_{z1}}{F_{y1}} + \frac{\Delta \theta_{z1}}{M_{z1}}, \quad (24)$$

$$B = \frac{\delta x_2}{F_{x1}} + \frac{\delta y_2}{F_{y1}} + \frac{\delta y_2}{M_{z1}}, \quad (25)$$

$$\beta = \frac{A}{B}, \quad (26)$$

where β represents the compliance–precision ratio. To reasonably and comprehensively consider the performance of flexure hinges, β can be used to assess the performance of flexure hinges.

In order to meet the practical application and have a basis for the selection of m , n , q , u , and d , it is necessary to study the influence of five parameters on β . When studying the influences of q and u on β , set $D = 15$ mm, $l = 30$ mm, and $d = 1$ mm, while q ranges from 0.5 to 3 and u ranges from 0.5 to 3.0. When studying the influences of m and n on β , set $q = 0.5$, $u = 3$, and $d = 1$ mm, while m ranges from 14 to 20 and n ranges from 18 to 24. When studying the influences

of d and n on β , set $q = 0.5$, $u = 3$, and $D = 15$ mm, while d ranges from 1.0 to 1.6 mm and n ranges from 18 to 24. Figure 8(a) shows that β decreased nonlinearly as q increased, whereas β increased nonlinearly as u increased. In addition, the sensitivity of β for parameter q increased as u increased, whereas the sensitivity of β on the parameter u decreased as increase q . In addition, according to the results, the effect of u on β was relatively greater than the effect of q on β , which indicates that parameter u had a greater influence on the performance of the flexure hinges. Figure 8(b) shows that β increased nonlinearly as m increased, whereas β decreased nonlinearly as n increased. Figure 8(c) shows that β decreased nonlinearly as d increased.

Based on the effects of five parameters on β , in order to study the performance of PTFH, a set of flexure hinge parameters were selected. $q = 0.5$, $u = 3$, $l = 30$ mm ($n = 19.1$), $D = 15$ mm ($m = 13.66$), and $d = 1.5$ mm.

E. Comparison of the PTFH and conventional flexure hinges

Generally, circular, elliptical, and parabolic are the conventional types of flexure hinges. Therefore, the β values of three typical bending hinges were compared with those of the PTFH. To make the comparison fair, for PTFH, q was set to 0.5 and u was set to 3,

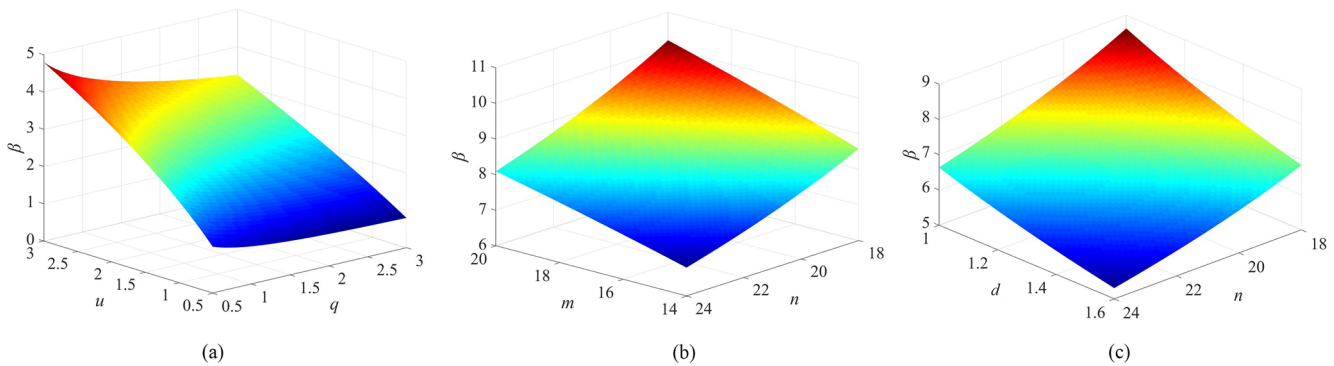


FIG. 8. Influence of geometric parameters on β of PTFHs. (a) q and u . (b) m and n . (c) d and n .

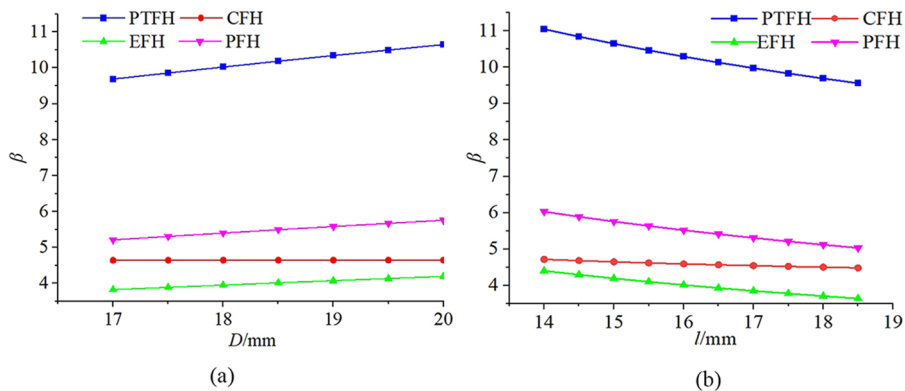


FIG. 9. Comparison results of the PTFH and other flexure. (a) Change of β with respect to D . (b) Change of β with respect to l .

and for all hinges, minimum thickness d was set to 1.5 mm. When parameter D is set to 20 mm, parameters l for all hinges ranged from 14 to 18.5 mm. When parameter l is set to 30 mm, parameters D for all hinges ranged from 14 to 18.5 mm, respectively. The resulting comparison results are shown in Fig. 9, where CFH, EFH, and PFH represent the circular flexure hinge, elliptical flexure hinge, and parabolic flexure hinge, respectively.

Figure 9 shows that when l was kept constant and D was changed, β increased nonlinearly as D increased. The β value of the PTFH was 118.97% that of CFH, 153.5% that of EFH, and 85.35% that of PFH. When D was kept constant and l was changed, β decreased nonlinearly as l increased. The β value of the PTFH was 123.3% that of CFH, 156.7% that of EFH, and 86.6% that of PFH. To summarize, when β was introduced to assess the performance of flexure hinges, the PTFH outperformed CFH, EFH, and PFH,

which means that the comprehensive performance of the PTFH in terms of compliance and rotation precision was superior to that of the conventional hinge forms.

IV. STRENGTH ANALYSIS AND DISPLACEMENT SPACE ANALYSIS

To obtain the working space of the PTFHs, one end of the entire flexure hinge was fixed, and a force or torque was applied along the z -direction or y -direction at the bolt hole. FEA showed that when a force of 9.9 N or a torque of 297 N mm was applied, the stress at the thinnest part of the hinge reached the elastic limit of the material (850 Mpa). As such, the working space was 1.2 mm, as illustrated in Fig. 10.

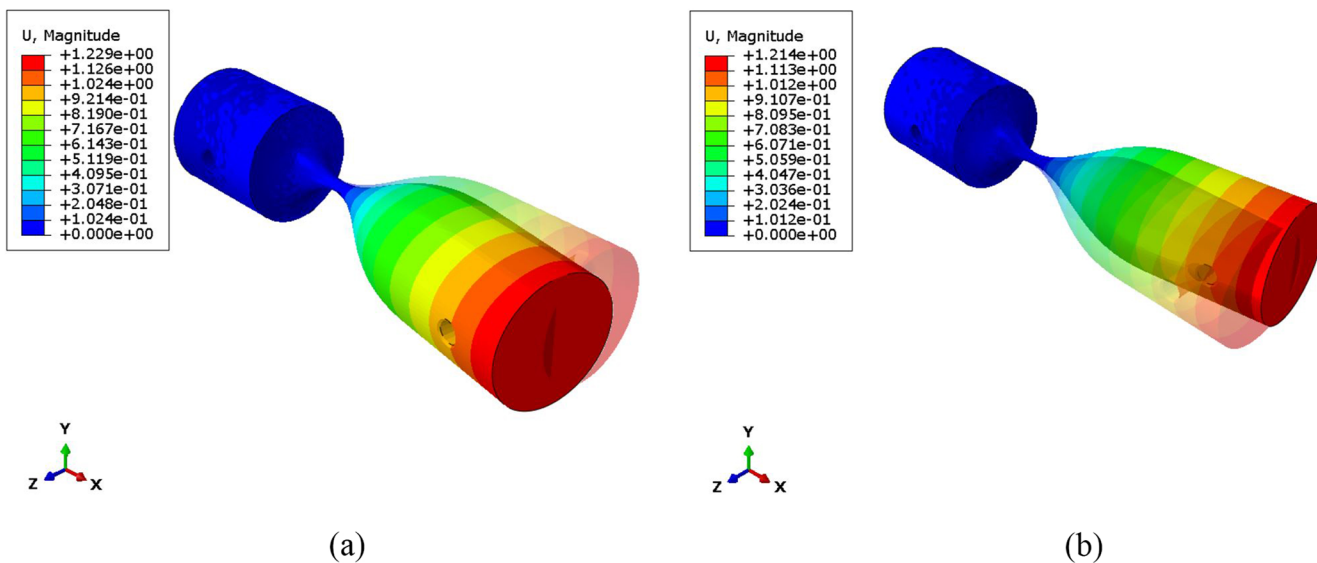


FIG. 10. Displacement result of static load and static moment. (a) Static load and (b) static moment.

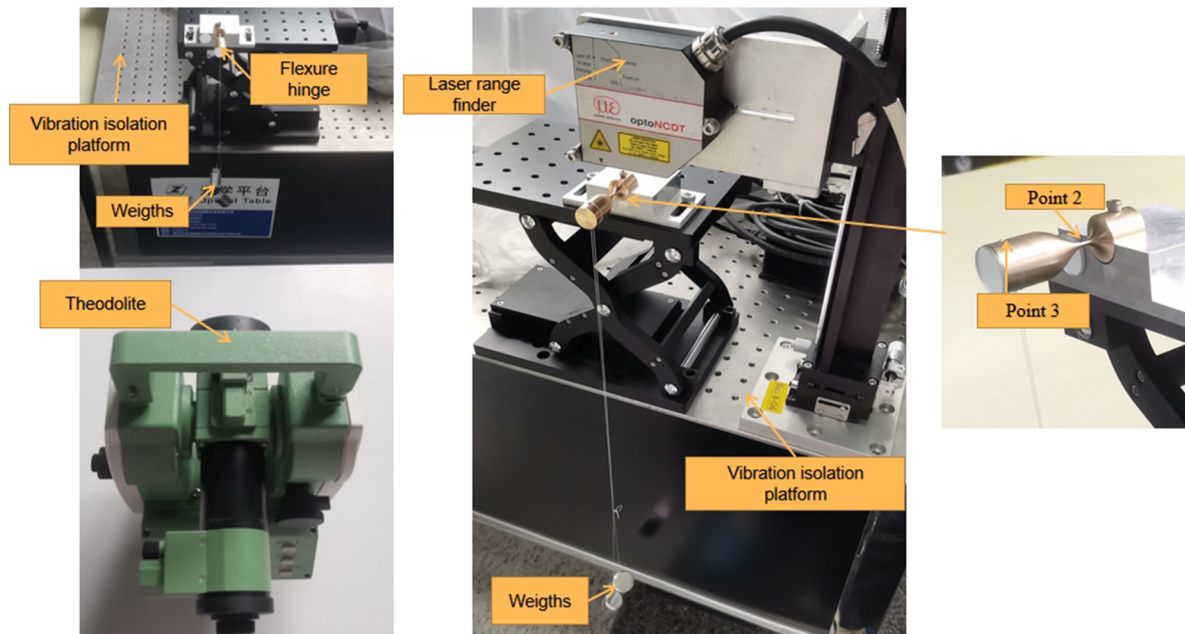


FIG. 11. Test system.

V. EXPERIMENT

The accuracy of the equation and the optimization results obtained from a simulation were verified. Figure 11 shows the test system of the processed flexure hinge model. The tolerance was ± 0.02 mm. The processing method was as follows: a beryllium bronze (QBe2.0) cylinder was cut according to the hinge curve using a computerized numerical control machine tool. Heat treatment was used to increase the elasticity and strength of the hinge (heated to 780°C , constant temperature for 120 min). A test system was established, which was mainly composed of a vibration isolation platform, laser range finder, and theodolite, as shown in Fig. 11. The parameter specifications of the theodolite were 1° field of view, $1''$ angle

measurement, and $0.1''$ minimum display. The parameter specifications of the laser range finder were a linear measuring range of 2 mm, an absolute error of $0.6\ \mu\text{m}$, and a resolution of $0.03\ \mu\text{m}$. The precise experimental method was as follows: A composite load (including torque around the z axis and tensile force along the y axis) was applied at the free end of the hinge. A metal weight with a mass of M was suspended on the upper fixture. The mass range of the weight was from 100 to 600 g, with increments of 100 g. The rotation angle of the PTFH was measured using a theodolite. All experimental equipment was placed on an air-floating isolation platform to isolate external vibrations.

As shown in Fig. 12, for the theoretical value of the displacement and rotation angle at point 3 and the displacement at point

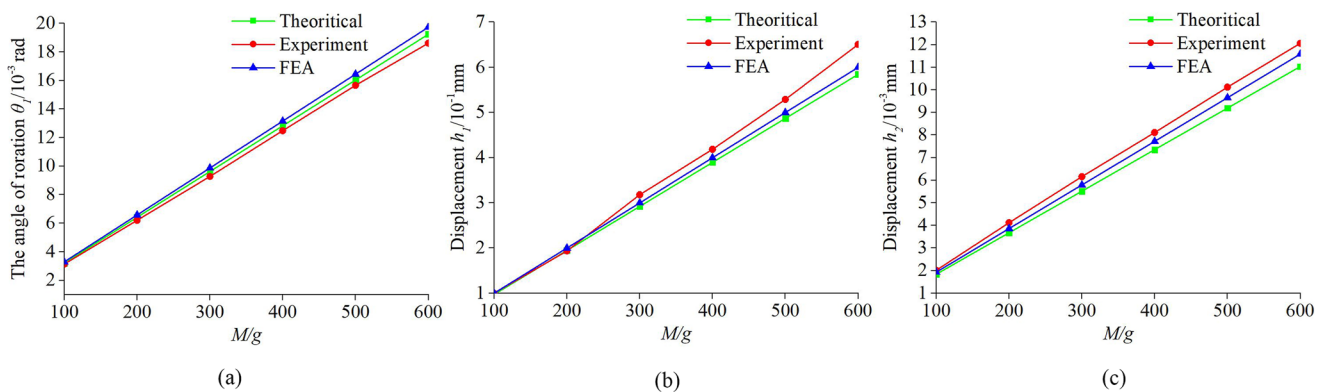


FIG. 12. Comparisons of experimental, FEA, and theoretical results. (a) The angle of rotation of point 3. (b) Displacement of point 3. (c) Displacement of point 2.

2, the FEA value, and the results for the experimental value, the relative error was less than 10% and the maximum relative error was ~9.4%. The error may have been caused by the following: the simplified analysis of the hinge model in the theoretical calculation, and the type and size of the grid affected the results of the analysis. In the final experiment, the error caused by the positioning of the model and the measuring equipment affected the final experimental results.

VI. CONCLUSIONS

In this paper, a new flexure hinge model called PTFHs was proposed. The degree of the power function q and degree of the trigonometric function u in the curve function were changed, which obtained different notch types of flexure hinges to meet the needs of flexure hinges in different scenarios. First, the influence of the degree of power function, degree of trigonometric function, and other parameters on the structure of the curve were analyzed. Then, based on Castigliano's second theorem, compliance and rotation precision equations were derived. The correctness of the theoretical formulas was verified by comparing the results of FEA and theoretical analysis, which had a maximum deviation of less than 8.5%. Furthermore, the influence of the flexure hinge parameters m , n , q , and u on compliance and rotation precision was analyzed. Compliance and rotation precision decreased nonlinearly as parameter m increased, and compliance and rotation precision increased nonlinearly as parameter n increased. In addition, parameter m had a greater effect on compliance and rotation precision than parameter n . When β was introduced, the conclusion of the analysis was that β decreased nonlinearly with an increase in q and increased nonlinearly with an increase in u , β increased nonlinearly with an increase in m and decreased nonlinearly with an increase in n , and β decreased nonlinearly with an increase in d . In addition, parameter q had a greater effect on β than parameter u . Then, the compliance-accuracy ratio β was calculated for circular, parabolic, and elliptical flexure hinges. The performance comparison of the flexure hinges was conducted. The results showed that the PTFH had a higher compliance-precision ratio β and better comprehensive performance. Next, a static analysis of the hinge was performed and its maximum working range was analyzed. Finally, a test system for measuring the rotation angle of the bending hinge was established. The experimental results were in basic agreement with the theoretical and finite element results. The relative error was less than 10%, and the maximum relative error was ~9.4%.

ACKNOWLEDGMENTS

The authors acknowledge the Chinese Academy of Sciences Key Laboratory of On-orbit Manufacturing and Integration for Space Optics System for support.

AUTHOR DECLARATIONS

Conflict of Interest

The authors have no conflicts to disclose.

Author Contributions

Jiabiao Li: Conceptualization (equal); Data curation (equal); Formal analysis (equal); Investigation (equal); Methodology (equal); Resources (equal); Software (equal); Supervision (equal); Validation (equal); Visualization (equal); Writing – original draft (equal); Writing – review & editing (equal). **Yang Zhao:** Conceptualization (equal); Supervision (equal); Validation (equal); Writing – review & editing (equal). **Qingwen Wu:** Conceptualization (equal); Investigation (equal); Methodology (equal); Resources (lead); Writing – review & editing (equal). **Peng Yu:** Investigation (equal); Methodology (equal); Resources (equal); Validation (equal). **Kai Zhang:** Investigation (equal); Methodology (equal); Resources (equal); Validation (equal). **Along Mao:** Investigation (equal); Methodology (equal); Resources (equal); Validation (equal).

DATA AVAILABILITY

The data that support the findings of this study are available from the corresponding author upon reasonable request.

REFERENCES

- 1 R. Shi, W. Dong, and Z. Du, *Rev. Sci. Instrum.* **84**, 075005 (2013).
- 2 L. Li, D. Zhang, S. Guo, and H. Qu, *Mech. Mach. Theory* **131**, 300 (2019).
- 3 M. Verotti, R. Crescenzi, M. Balucani, and N. P. Belfiore, *J. Mech. Des.* **137**, 012301 (2015).
- 4 K. Chandrasekaran and A. Thondiyath, *J. Med. Devices* **11**, 014502 (2017).
- 5 J. Wu, Y. Zhang, Y. Lu, Z. Wen, D. Bin, and J. Tan, *Rev. Sci. Instrum.* **89**, 045010 (2018).
- 6 S. Du, J. Liu, H. Bu, and L. Zhang, *Rev. Sci. Instrum.* **91**, 035121 (2020).
- 7 W. Ma, R. Wang, X. Zhou, and G. Meng, *Proc. Inst. Mech. Eng., Part C* **234**, 1859 (2020).
- 8 X. Sun, B. Yang, Y. Gao, and Y. Yang, *Robot. Comput.-Integr. Manuf.* **66**, 101988 (2020).
- 9 P. Wang and Q. Xu, *Mech. Mach. Theory* **108**, 1 (2017).
- 10 N. Chen and C. Tian, *Sens. Actuators, A* **323**, 112660 (2021).
- 11 M. N. M. Zubir and B. Shirinzadeh, *Precis. Eng.* **33**, 362 (2009).
- 12 Y. Tian, C. Zhou, F. Wang, K. Lu, and D. Zhang, *Sens. Actuators, A* **309**, 112027 (2020).
- 13 P. Schmitt and M. Hoffmann, *J. Microelectromech. Syst.* **29**, 214 (2020).
- 14 H. Yun, L. Liu, Q. Li, W. Li, and L. Tang, *Mech. Syst. Signal Process.* **127**, 328 (2019).
- 15 L.-J. Lai and Z.-N. Zhu, *Sens. Actuators, A* **266**, 122 (2017).
- 16 J. Wen, N. Wan, R. Wang, S. Chen, J. Zheng, and J. Li, *IEEE Access* **7**, 25908 (2019).
- 17 J. Yu, G. Hao, G. Chen, and S. Bi, *J. Mech. Eng.* **51**, 53 (2015).
- 18 L. X. Hui, G. Lei, W. Yan, S. Haoran, and H. Yong, *J. Magn. Magn. Mater.* **556**, 169415 (2022).
- 19 J. Paros, *Mach. Des.* **37**, 151 (1965).
- 20 N. Lobontiu, J. S. Paine, E. Garcia, and M. Goldfarb, *Mech. Mach. Theory* **37**, 477 (2002).
- 21 Y. Tian, B. Shirinzadeh, and D. Zhang, *Precis. Eng.* **34**, 408 (2010).
- 22 R. Lin, X. Zhang, X. Long, and S. Fatikow, *Rev. Sci. Instrum.* **84**, 085004 (2013).
- 23 M. Liu, X. Zhang, and S. Fatikow, *Rev. Sci. Instrum.* **87**, 055106 (2016).
- 24 Q. Li, C. Pan, and X. Xu, *Precis. Eng.* **37**, 135 (2013).
- 25 H. Wei, B. Shirinzadeh, H. Tang, and X. Niu, *Mech. Mach. Theory* **156**, 104154 (2021).
- 26 R. Wang, X. Zhou, and Z. Zhu, *Rev. Sci. Instrum.* **84**, 095008 (2013).
- 27 J. Wu, Y. Zhang, S. Cai, and J. Cui, *Mech. Mach. Theory* **128**, 560 (2018).

²⁸G. Chen, X. Shao, and X. Huang, *Rev. Sci. Instrum.* **79**, 095103 (2008).

²⁹J. Kong, Z. Huang, X. Xian, Y. Wang, and P. Yu, *Sci. Prog.* **103**, 1–26 (2020).

³⁰L. Li, D. Zhang, H. Qu, and Y. Wang, *Mech. Mach. Theory* **169**, 104677 (2022).

³¹H. Wei, J. Yang, F. Wu, X. Niu, and B. Shirinzadeh, *Precis. Eng.* **76**, 294 (2022).

³²M. Ling, L. Yuan, and X. Zhang, *Precis. Eng.* **81**, 124 (2023).

³³K. Li, X.-L. Gao, and A. Roy, *Compos. Sci. Technol.* **63**, 1769 (2003).

³⁴A. Farrokhhabadi, M. M. Ashrafian, and M. Fotouhi, *J. Sandwich Struct. Mater.*

24, 1726 (2022).